Available online at www.sciencedirect.com
ScienceDirect
Journal of the European Ceramic Society 27 (2007) 1035–1040
www.elsevier.com/locate/jeurceramsoc

Local current measurement in a solid oxide fuel cell repeat element

Frédéric Ravussin, Jan Van herle *, Nordahl Autissier, Michele Molinelli, Diego Larrain, Daniel Favrat

Laboratory of Industrial Energy Systems (LENI), ME A2 Station 9, Faculty of Engineering (STI), Ecole Polytechnique Fédérale de Lausanne, (EPFL), CH-1015 Lausanne, Switzerland

Available online 15 June 2006

Abstract

A planar solid oxide fuel cell repeating unit, 50 cm^2 in total active electrode size, consisting of an anode supported electrolyte cell bearing two 7 mm holes for fuel and air injection, and contacted to two dense metal current collector plates via gas distribution layers, was constructed with the aim of measuring local current densities rather than the integral current over the full area. The cathode side was entirely segmented (i.e. cathode layer, gas distribution layer, metal current collector plate) into eight galvanically separated parts of ca. 6.5 cm^2 each, with own current and potential leads.

The element was characterised at 750–800 °C and different H_2 fuel flows, by total and local current–voltage recording as well as by local electrochemical impedance measurement. The segment that incorporates the fuel injection hole for the whole cell always outperforms all other segments, the corner segments furthest away from the fuel injection perform least. Differences in local potential can be higher than 200 mV. Polarizing one segment individually and recording the change in potential of the other segments reveals the different contributions of convection and diffusion on the flow field. Contrarily to small ideal single cells, total performance of such larger sized, stackable cells is decisively governed by the distribution fields and their weakest zones.

Keywords: Interfaces; Impedance; Fuel cells; Non-destructive evaluation; Resolved current density

1. Introduction

To circulate useful d.c. current on the order of several 10 A, planar solid oxide fuel cells (SOFC) are several 10 cm^2 in size. In stacked condition, i.e. with series connection of several cells as so-called repeat elements, the necessary presence of fuel and air injection zones to each cell and of evacuation zones for oxidized fuel products and air excess from each cell leads to flow inhomogeneity at each cathode and anode, depending on flow magnitude and pressure drop together with the particular geometry under study. This flow inhomogeneity leads to a distribution field of current density, temperature and ultimately stress and therefore co-determines the operational reliability of the fuel cell. Also, it can lead to low local cell potential (i.e. high local pO_2 at the anode) causing the nickel anode to reoxidize to nickel oxide, accompanied by high risk of cell fracturing.[1]

The distribution fields can be numerically predicted, e.g. using computational fluid dynamics,[2] based on initial assumptions for the electrochemical reaction model. These computed results need to be compared with experiment, for validation and confirmation purposes.

Few attempts[3–5] have been reported to locally assess current density in fuel cells, primarily for the low temperature polymer electrolyte type, PEFC. Kucernak et al.[5] performed space-resolved current–voltage measurement along a single channel, low temperature PEFC element, from which optimal anode feeding could be derived. In SOFCs, Metzger[6] measures simultaneously the fields of concentration, current density and temperature within a 74 cm^2 repeat element. The segmentation of the cell was in 16 equal squares 4.6 cm^2 each. Due to insufficient quality of the electrolyte support cells (leakage through the electrolyte, contacting problems), sometimes ill-explainable temperature values were recorded. The leaky electrolytes imposed the use of large gas flows, implying low fuel conversion and low efficiency; little variation in local gas compositions was measured. Gas analysis was performed off-line via gas chromatography.

Compared to the considerable theoretical effort produced to date (simulation of distribution fields), such attempts to obtain real-time experimental data on the repeat element (i.e. stack-like) level remain few. The knowledge of these data is crucial,

* Corresponding author. Tel.: +41 21 693 35 10; fax: +41 21 693 35 02.
E-mail address: Jan.Vanherle@epfl.ch (J. Van herle).

0955-2219/$ – see front matter © 2006 Elsevier Ltd. All rights reserved.
doi:10.1016/j.jeurceramsoc.2006.05.089

first in order to validate the simulations, and second to use the simulation model as a tool for design optimisation of the fuel cell.[7]

The paper presents results on local current density measurement in a SOFC repeat element, i.e. including the cell and both current collectors.

2. Experimental

The cell is of 50 cm^2 active area size and based on tape cast, 0.01 mm thin yttria-doped zirconia (YSZ) electrolyte supported on a Ni-zirconia anode (80 mm × 80 mm × 0.25 mm). The cathode, $LaSrFeO_3$, was screenprinted (0.03 mm thick), sintered and segmented in eight galvanically separated rectangles, according to the sketch in Fig. 1. Current collection on both electrodes is achieved with a dense ferritic steel sheet (0.75 mm thick); gas distribution layers GDL (0.5–1 mm thick) are intercalated between the metal and the electrodes.[8] The cathodic metal sheet and GDL were equally segmented according to the geometry of Fig. 1. These individual segments were glued on a 64 cm^2 mica sheet, ceramic paste was applied between adjacent segments (1 mm apart) to ensure their separation. The anode side was left unaltered compared to a regular, i.e. unsegmented, cell element. Each cathode current collector carried individual current and potential leads. The assembly (view on the cathode) is shown in Fig. 2. Fuel and air are injected via the inlet holes in segments #2 and #7, respectively. Thus the flow lines are mainly in counter flow configuration, air flowing out behind segments 1–3 and fuel flowing out behind segments 6–8. No glass seal is used, but instead a diffusion barrier ring around the inlet holes (on one face of the cell only) and a diffusion barrier border along the three cell edges forming a U-shape around the inlet holes. The assembly was spring-compressed between Inconel housing flanges (using mica sheets for electrical insulation) equiped with gas feed tubes, and placed in a chamber furnace. The SOFC repeat element was characterised at 750–800 °C and different H_2 fuel flows, 180, 260 and 400 ml/min as indicated by a rotameter (ball-floating type). Air flow was in stoichiometric oxygen excess of 2.5 with

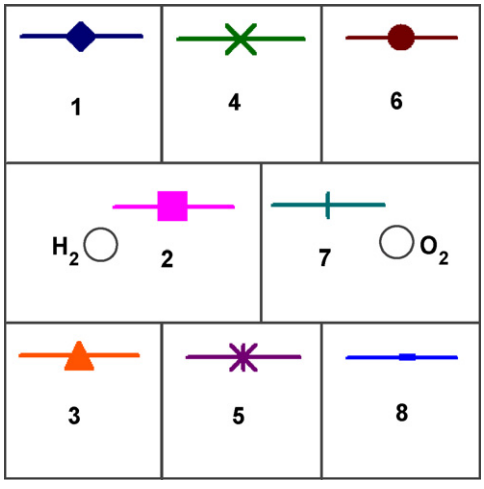

Fig. 1. Schematic drawing of the segmented SOFC. Numbering and symbols of the segments are consistently used throughout the text and figures.

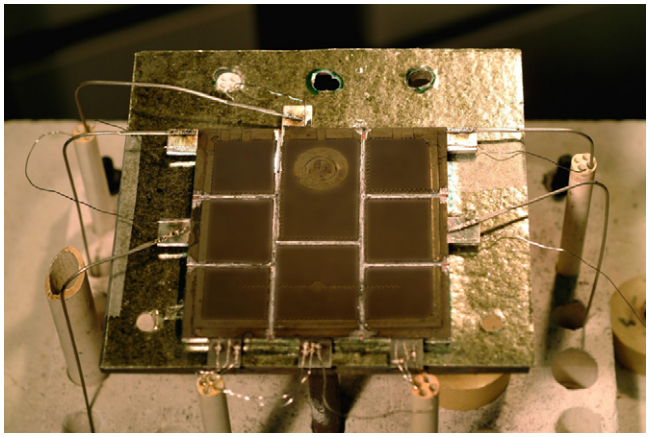

Fig. 2. Segmented SOFC assembly seen on the cathode.

respect to fuel. Though equipped with a gas-specific flow scale for a set inlet pressure (which was respected), separate post-calibration of the rotameters with an accurate flowmeter showed deviations of the nominal flows by as much as +30%. Nonetheless, flows will be given in the paper by these nominal values. For electrical characterisation, the cell was connected to instrumentation from Zahner Elektrik (D). All segment leads went into a power multiplexer box (P-MUX), itself interfaced to a power potentiostat (PP240, 40 A, 5 V) and a base control unit, IM6. The latter contained an internal potentiostat (max. 3 A) and a frequency response analyser for electrochemical impedance measurement (EIS). For current–voltage recording, one segment could be electrically decoupled from the remaining seven segments: the former was then controlled by the internal potentiostat, and the latter jointly by the power potentiostat PP240. The same circuitry allowed to perform segment-per-segment EIS recording.

3. Results

3.1. Comparison with unsegmented cell

Fig. 3 shows the total current–voltage (i–V) characteristic, at 800 °C and the three employed fuel flows, for the segmented cell (all eight segments active) compared to an unsegmented cell prepared from the same batch. In principle, responses for both cells should be identical. Some differences are apparent: open circuit voltage (OCV) for the regular (unsegmented) cell is lower, but its slope (approximated as apparent area-specific resistance, ASR ($\Omega\,cm^2$)) is lower too. It could not be clearly established whether these differences were cell-intrinsic or due to the test arrangement. Performance differences between nominally identical cells from the same production batch have experimentally frequently been found in our Laboratory, easily 30 mV in OCV and ± 20% in ASR. Given that the segmented cell response is not far off these variations (OCV ca. 40 mV higher, ASR ca. 25% higher), it can reasonably be assumed that the measurement disturbance, introduced by the segmentation, is not major and that therefore the segmented test arrangement is validated for the subsequent results.

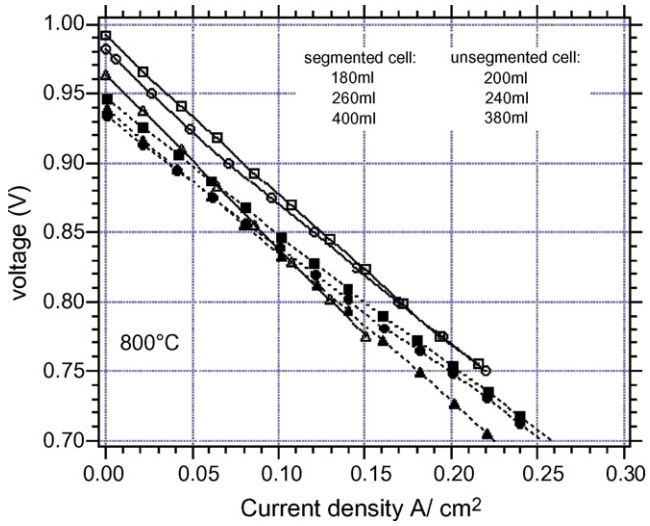

Fig. 3. Total *i–V* response of the segmented cell (open symbols) compared with an unsegmented cell (closed symbols) of the same batch, at 800 °C and similar H_2 gas flows.

3.2. Local i–V

Fig. 4 shows a typical plot of local *i–V* (here for 800 °C, H_2 flow 260 ml/min), i.e. the individual *i–V* taken on each segment (internal potentiostat) while all other segments also carry a meaningful current (total of 8 A or ca. 0.17 A/cm^2). Segment #2 (located at the fuel inlet) clearly outperforms all others. It is followed by segment #7, located at the air inlet and directly downstream from the fuel inlet. Segments #1–3, #4–5 and #6–8 should in principle show a pairwise identical behaviour, if the flowfield were ideally symmetric and the contact assembly ideally mounted. Clearly this is not the case: segments #1–4–6 ("up" from segment #2) systematically showed superior behaviour to segments #3–5–8 ("down" from segment #2). The asymetric response must arise from problems in the test arrangement (non-planarity of a partial contact, a sealing defect leading to a preferential flow orientation, or the like). Finally, segment #1 (and slightly segment #3) shows the onset of current limitation below 0.6 V. This is indicative of mass transport limitation and was typically observed for these inlet corner segments (#1 and #3), at low flow: indeed numerical simulation clearly predicts insufficient flooding to these corners.[2]

From Fig. 4, the local *i–V* per segment can reasonably well be approximated by its corresponding ASR value. These are given in Fig. 5a, as a function of total current circulating through the cell (on the other seven segments) and in Fig. 5b, as a function of fuel flow.

Fig. 5a shows the segment-ASR to be fairly independent from the current circulation elsewhere in the cell, at least up to 8 A or 170 mA/cm^2 (corresponding to low fuel conversion of ca. 20%). In reality (not shown here but later in Fig. 8), each local *i–V* exhibits a downwards parallel shift to a slightly lower potential, including at OCV, as total current on the cell increases.

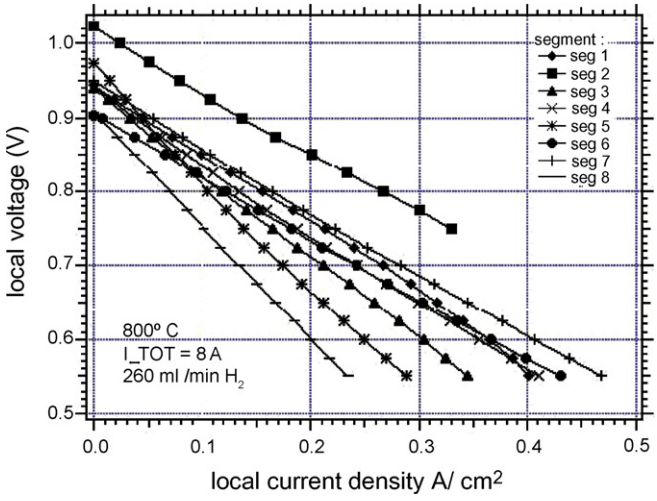

Fig. 4. Local *i–V* for each segment (#1 to #8) at 800 °C, 260 ml/min H_2 while the cell remainder (i.e. the sum of the other seven segments) carry a current of I_{tot} = 8 A (ca. 0.17 A/cm^2).

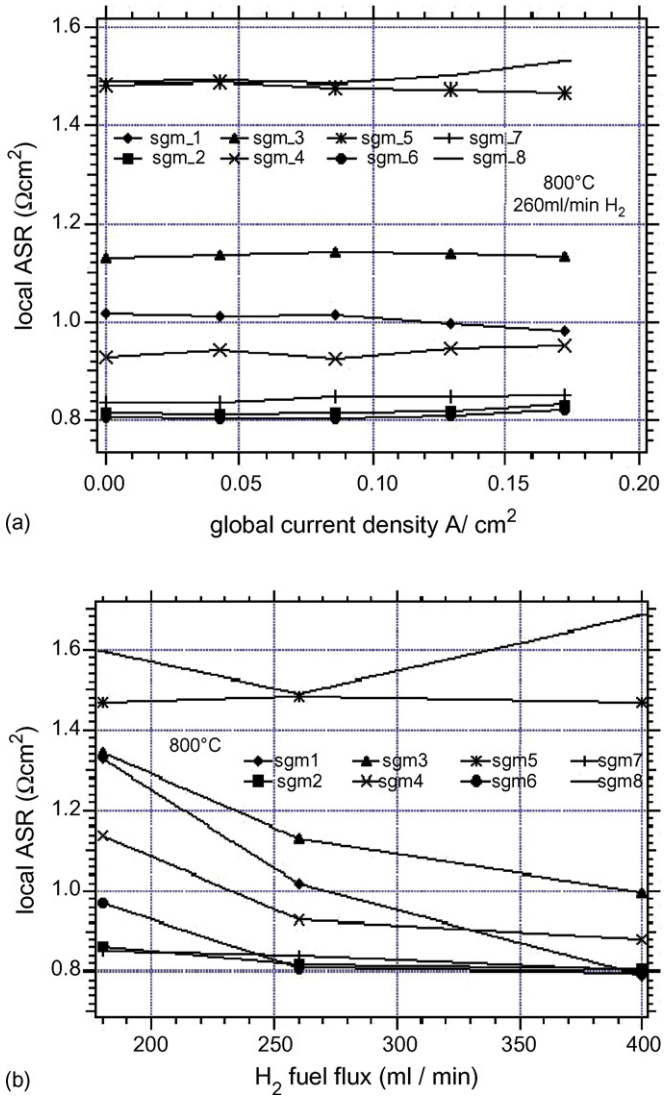

Fig. 5. Local ASR per segment, at 800 °C, as (a) a function of global current density (circulating on the other seven segments) and (b) as a function of total fuel flow.

Fig. 5b shows the segment-ASR to be clearly dependent upon flow. All ASR are expected to drop with increasing flow, as generally shown, in particular for the change from 180 to 260 ml/min. The effects on the inlet segments (#2 and #7) is smallest, as these are already well flooded even at the lowest flow. The effect of higher flow is largest on the inlet corner segments (#1 and #3). ASR values tend to homogenize (at least for five segments) at the largest flow. The unusual increase on segment 8 at largest flow points again to an anomaly in the test arrangement and to the fact that increased flow not necessarily floods the whole cell. In fact, optimal flow for this particular test seems achieved at around 300 ml/min H_2.

We find further confirmation of the observed behaviour when plotting OCV per segment as a function of flow, Fig. 6: highest for the fuel inlet and the cell center, lowest in the corners. All OCV obviously increase with flow, but flatten out already between 260 and 400 ml/min. Clearly theoretical Nernst potential (1.1 V) is not reached. In the present case, the potential lower than theoretical is explained by the combined effect of gas leakage (imperfect sealing, back-diffusion) and partial electronic shorting across the thin electrolyte,[2,7] where the former effect is mostly responsible for the OCV difference between lowest (180 ml/min) and intermediate (260 ml/min) flow.

3.3. Local electrical losses

A vast series of EIS measurements was conducted (as a function of temperature, flow, local and total *dc* bias), of which here only the summary can be given. Each EIS response typically displayed two semicircles, one for each electrode. Here we consider only the ohmic loss (high frequency intercept with the real axis, R_Ω, in a Nyquist diagramme) and the polarisation loss (low frequency intercept, R_{tot}, minus R_Ω). Fig. 7 plots these values for all segments at OCV, 800 °C and 260 ml/min H_2, normalised to the segment area (in $\Omega\,cm^2$). One would expect all normalised ohmic drops R_Ω to be equal. This is clearly not the case and reillustrates the importance of proper contacting homogeneously

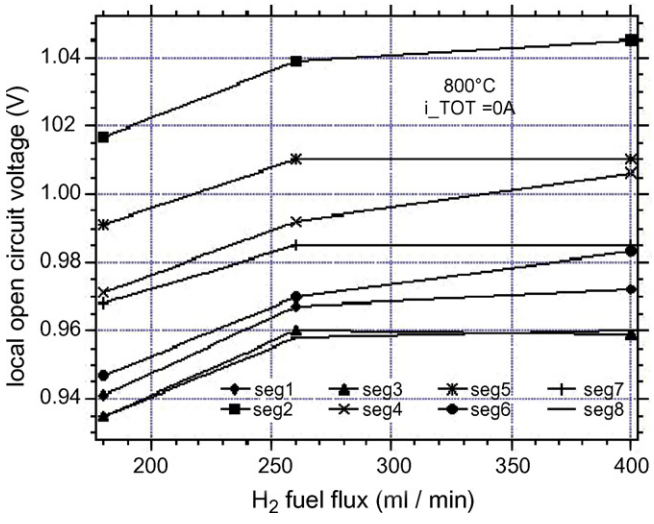

Fig. 6. Local open circuit voltage (OCV) per segment as a function of total fuel flow, 800 °C, global current density = 0 A/cm^2.

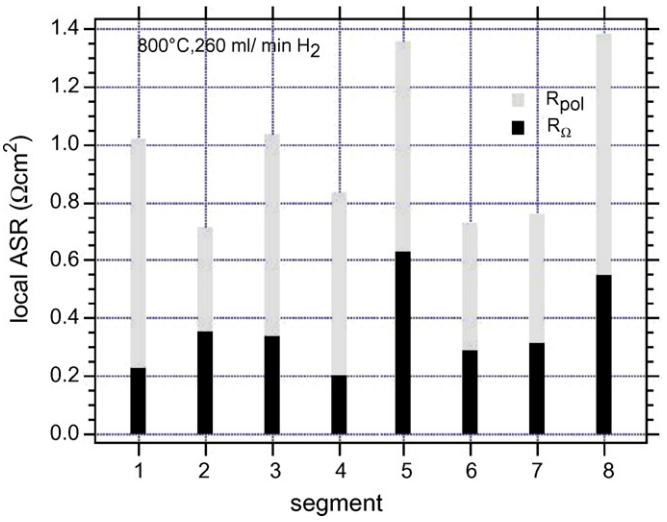

Fig. 7. Normalised local ASR per segment ($\Omega\,cm^2$), at open cicrcuit condition, 800 °C and 260 ml/min fuel flow, separated in ohmic (R_Ω) and polarisation resistance (R_{pol}), obtained from local impedance measurement.

over the whole cell. Values vary between 0.2 and as much as 0.6 $\Omega\,cm^2$; for small single cells using idealised Pt-mesh current collection (no ferritic steel, no GDL) a value of 0.1 $\Omega\,cm^2$ is typically obtained. The poor relative performance of segments #5 and #8 seen higher (Fig. 4) is at least partially explained from Fig. 7 by their abnormally high ohmic loss, likely because of insufficient contacting. This could not be clearly established at post-mortem disassembly. Polarisation loss, R_{pol}, here indicative for gas feed quality, also clearly reflects the recorded *i–V* behaviour: lowest for the inlet segments (#2 and #7) and the center segments #6 and #4, highest for the corner segments. The total losses R_{tot} per segment are entirely consistent with the ASR values given in Fig. 4, for the same conditions. (Overall, values in Fig. 7 lie about 0.1 $\Omega\,cm^2$ lower than in Fig. 4: this is explained by the fact that the cell performance typically improves with test duration due to cathode activation.[8] The test was run for over a month and *i–V* data and EIS data were recorded at different time intervals. This change in performance with time does not nullify data interpretation as it is homogeneous over the whole cell and relatively small (<15%).)

3.4. Local influences

A particularly useful outcome is the study of the influence of polarisation of one segment (via the internal potentiostat) on the local potential of the others, which was performed in both OCV and overall d.c. bias conditions. Here the effect on local OCV is discussed, which is more pronounced. The general aspect is given in Fig. 8, which displays OCV on each segment as a function of the current drawn on the rest of the cell (=all other seven segments). Clearly all local OCV drop with the cell current, as expected: water vapour is produced by the current, lowering the potential through the Nernst equation. The upstream segments for fuel inlet (#1–3) are somewhat less influenced than the downstream segments #4–8. Water vapour transport leading to local potential lowering can occur in two ways: convective

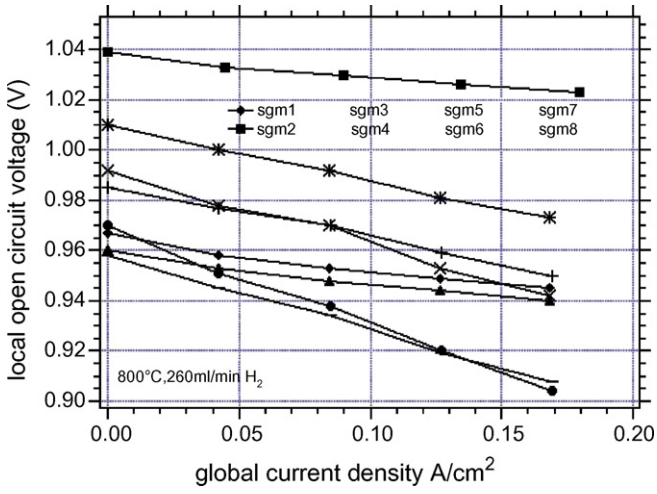

Fig. 8. Local OCV per segment as a function of global current density (=on all other segments combined), 800 °C, 260 ml/min fuel flow.

through the flow (pressure gradient driven), and diffusive (concentration gradient driven). Studying individual segments can quantify the contribution of both processes, as illustrated hereafter in Fig. 9. From Fig. 8, it is seen that the lowering of local OCV as a function of global current (drawn on the cell remainder) can be approximated by a straight line fit, in units of $\Omega\,cm^2$. Thus a value of $-0.1\,\Omega\,cm^2$ means that local OCV is lowered by 10 mV when globally 100 mA/cm^2 are drawn (on the other segments). This representation is used for plotting Fig. 9.

Fig. 9 shows the effect on local OCV when only one segment is polarised. When drawing current only on segment #1, clearly its downstream segments #4 and #6 are mostly affected (slope -0.18 and $-0.1\,\Omega\,cm^2$, respectively). When drawing current only on the fuel inlet segment #2, all other segments are more or less equally affected (average slope around $-0.075\,\Omega\,cm^2$).

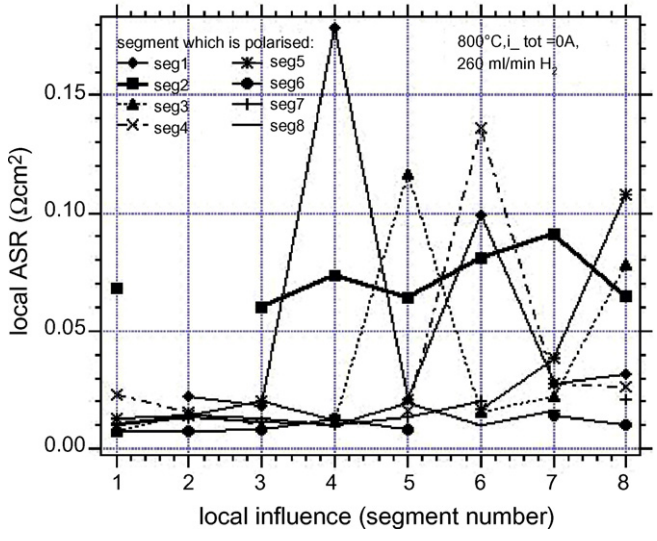

Fig. 9. Local ASR ($\Omega\,cm^2$) expressing the drop in OCV on one of seven segments (X-axis) as a function of the current density drawn on the remaining, eighth, segment (given by the legend), at 800 °C and 260 ml/min.

Finally, when drawing current on an "exit", e.g. segment #6 or #8, still OCV on the other segments is lowered (slope ca. $-0.02\,\Omega\,cm^2$), even though the water vapour produced locally at these exit segments should be transported out of the cell by convection (direction of the flow). This therefore evidences, to some extent quantitatively, diffusion transport inward to the cell.

Finally, comparison has been made between the experimentally determined local current density distribution and the numerically obtained current density distribution by computational fluid dynamics.[1,2] Qualitatively, agreement was satisfactory. Quantitatively, differences are explained by the asymmetry in the experimental values (simulation of course yields a perfectly symmetric flowfield) and by the underestimation of leakage in modeling. The latter is now added to the model, accounting for imperfect sealing, and amply confirmed by local concentration measurement in a separate test arrangement. This will be reported elsewhere.

4. Conclusion and outlook

A segmented solid oxide fuel cell repeat element (50 cm^2 total) was designed for measuring local current density (eight segments of each ca. 6.5 cm^2). Local current–voltage and local impedance (i.e. for each segment) could be measured as a function of operating conditions (temperature, flow, d.c. bias, with other segments active or not). A clear picture of the flow field was obtained for the presently used cell configuration. This was limited especially in the corner areas, due to the counterflow arrangement with punctual inlets. A new, modified, cell configuration is redesigned based on these results, which will overcome the identified limitations.

Acknowledgements

Sincere acknowledgements for financial support are expressed to the Swiss National Science Foundation (contract 200021-100721/1), the Swiss Commission for Technology and Innovation (contract 6649.3 IWS-IW) and the Swiss Federal Energy Office (contract 86895), as well as to HTceramix S.A. (Yverdon, Switzerland) for supply of the SOFC components.

References

1. Van herle, J., Larrain, D., Autissier, N., Wuillemin, Z., Molinelli, M. and Favrat, D., Modeling and experimental validation of SOFC materials and stacks. *J. Eur. Ceram. Soc.*, 2005, **25**, 2627–2632.
2. Autissier, N., Larrain, D., Van herle, J. and Favrat, D., CFD simulation tool for SOFC. *J. Power Sources*, 2004, **131**, 313–319.
3. Bender, G., Wilson, M. S. and Zawodzinski, T. A., Further refinements in the segmented cell approach to diagnosing performance in polymer electrolyte fuel cells. *J. Power Sources*, 2003, **123**, 163.
4. Mench, M. M., Wang, C. Y. and Ishikawa, M., In situ current distribution mesurements in polymer electrolyte fuel cells. *J. Electrochem. Soc.*, 2003, **150**(8), A, 1052.
5. Kulikovsky, A. A., Kucernak, A. and Kornyshev, A. A., Feeding PEM fuel cells. *Electrochim. Acta*, 2005, **50**(6), 1323–1333.
6. Metzger, P., Schiller, G. and Störmer, A., SOFC characteristics along the flow path. In *Proceedings of the sixth European solid oxide fuel cell*

forum, Vol. 2, Lucerne (CH), ed. Mogens Mogensen, European Fuel cell Forum Sekretariat, CH-5452 Oberrohrdorf, Switzerland, 2004, pp. 989–999.

7. Larrain, D., Autissier, N., Maréchal, F., Van herle, J. and Favrat, D., Generalized model of planar SOFC repeat element for design optimisation. *J. Power Sources*, 2004, **131**, 304–312.
8. Molinelli, M., Larrain, D., Ihringer, R., Constantin, L., Autissier, N., Bucheli, O. *et al*., Current collection and stacking of anode support cells with metal interconnects to compact repeating units. In: *Proceedings of the eighth international symposium on solid oxide fuel cells*, Paris (F), ed. S. Singhal and M. Dokiya. The Electrochemical Society Inc., Pennington, New York, 2003, Proceedings volume PV-2003-07, pp. 905–913.